Time-resolved microscopy with femtosecond few-electron pulses.

Contact *w.a.bryan@swansea.ac.uk*

W. A. Bryan and C. W. Barlow-Myers
*Department of Physics, College of Science,
Swansea University, Singleton Park,
Swansea, SA2 8PP.*

A. R. Bainbridge
*Accelerator Science and Technology Centre,
STFC Daresbury Laboratory, Daresbury Science and
Innovation Centre, Keckwick Lane, Daresbury,
Cheshire WA4 4AD.*

Introduction

The ultrafast laser community is well versed in the concept of time-resolved measurement of rapidly evolving systems through pump-probe observation. Employing one laser pulse to pump a system, be it an electronic transition in an atom, a vibrational or rotational excitation in a small chemical system, a conformation change in a biological system or a phase change in a solid state initiates a temporal evolution which is probed a varying time later with a second laser pulse. Carefully selecting the wavelength, duration, intensity and phase characteristics of the pump and probe, in some cases independently, is the cornerstone of a swathe of modern laser physics.

The observable in such measurements is either reflected in a modification of the probe pulse photons, or through a change in an additional quantity, be it through mass and energy resolved spectroscopy of emitted photons, ions or electrons, electrical properties, temperature or acoustic information. This is a non-exhaustive list however highlights the need for infernal of intermediate and final states when performing such observations. Moreover, pump-probe measurements carried out with light are generally confined by the wavelength of the radiation used, thereby are inherently prevented from accessing spatial information on the atomic scale.

Electron microscopy has no such limitation in terms of wavelength. The well-known de Broglie wavelength of the electron is, as a consequence of the mass of the particle, significantly smaller than its photonic counterpart in terms of energy. This led to transmission electron microscopy, which is now able to spatially resolve on the atomic scale, and the numerous tip-enhanced forms of observation, which can in some cases be coupled with photonic excitation.

Nonetheless, only recently has the technology existed to simultaneously observe on ultrafast (femtosecond) timescales while maintaining spatial information [1-10]. Creating femtosecond pulses of coherent or quasi-coherent electrons has been achieved using relatively common laser systems driving either work-function actuated thin film metal sources (e.g. gold driven by UV photoemission) [1,2] or nanoscale metal tips (NSMTs) [5-7] which, due to the field enhancement afforded by the nanometric radius of curvature of the NSMT apex, act in a manner similar to single atoms exposed to femtosecond laser pulses. The combined electric field of the incident laser pulse and the subsequent field enhancement facilitate the tunneling of electrons at or near the Fermi level directly into the continuum through two or more photon absorption. It is the nonlinear nature of this emission that limits the duration of the resulting electron pulse to less than that of the drive laser pulse.

While a number of headline observations have been made with femtosecond electron diffraction or microscopy [1,4,5,10], a number of experimental hurdles still exist. Firstly, unless they are formed of on average one electron or less, space-charge (SC) causes dispersion of such pulses even in vacuum [10]. This counteracts one of the major advantages of using electrons for imaging – typical scattering cross sections are five orders of magnitude larger than photons of the same energy [2]. A number of concepts have been proposed to overcome this, ranging from acceleration to relativistic energies whereby the transit time between source and target is contracted, to RF compression which modifies the momentum distribution of the electron pulse as it propagates such that it is minimized at the target [see 2 and references therein for full discussion]. Both allow the delivery of $\sim 10^5$ electrons in one pulse hence making single-shot imaging possible. The simplest solution however is to operate in a regime where one electron is emitted at a time, negating SC effects. This does however place a requirement on the process being studied, in that it must be recoverable and repeatable.

This then brings us to the second major hurdle, in that as compared to ultrafast pulses of photons, measuring the duration of electron pulses is extremely difficult. The scattering of electrons by the ponderomotive force has been explored with some success however it appears to be limited to at best tens of picoseconds [2,4]. Laser-initiated streaking has been attempted with similar results.

In the present work, we make use of two NSMTs [7], one as a source and the second as a target. This system was chosen as it potentially has a very fast response to applied laser light, and at low electron energies, can result in significant scattering, making the measurement of small fluxes possible.

Experimental

A schematic of our experiment is presented in figure 1. Two tungsten NSMTs are employed, with the axis of the "source"
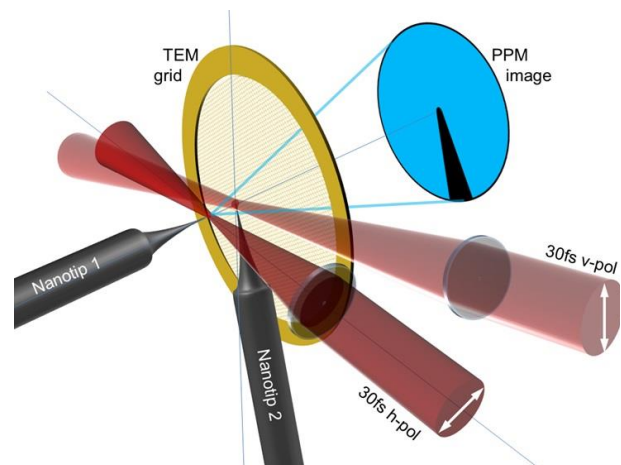
Figure 1. Schematic of femtosecond electron microscopy experiment. Nanotip 1 (NSMT1) is illuminated with a 30 fs 800 nm pulse from UFL1 operating at 50kHz. The pulse energy into the focus is < 1 µJ however the field enhancement around the apex facilitates electron emission. A voltage of 300 V applied between NSMT 1 and the TEM grid 0.4 mm distant accelerates the electrons past NSMT2. As the delay between the two laser pulses is scanned, the electron pulse probes the reaction of NSMT to the laser field. The resulting distribution of electrons is detected on a microchannel plate and phosphor screen detector.
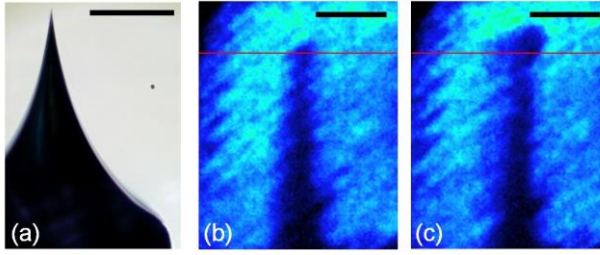
Figure 2. (a) Optical microscope image of NSMT2. Scale bar is 100 microns. (b) fs-ePPM image of NSMT2 at a delay of -2 ps, hence the electron pulse passes before excitation of the second nanotip. (c) fs-ePPM image of NSMT2 at a delay of +2 ps, illustrating the influence of the probe laser pulse on NSMT2 and hence on the passing electron pulse. In the case of (b) and (c), the laser pulse arrives from the left and the shape of the charge plume is governed by optical diffraction, and the scale bar is 5 microns.

NSMT pointing at the apex of the "target" NSMT. Sub-30 fs laser pulses at 800 nm are generated by the UFL1 laser system from the EPSRC Laser Loan Pool. This system consists a Light Conversion Pharos optically pumping an Orpheus-N non-

collinear optical parametric amplifier. Pulse compression is performed with a prism compressor configured to compress following propagation through 8 mm of fused silica, and full spectral and temporal reconstruction is managed with a custom-built FROG.

Splitting and focusing the output of UFL1 onto NSMT1 initiates femtosecond electron emission on the condition that the laser polarization is along the axis of the tip. Furthermore, the spot size at the apex must be small to prevent thermionic emission. NSMT2 is also illuminated by the second split of UFL1 and a translation stage allows the delay between the two laser pulses to be controlled with few-fs accuracy.

By placing NSMT2 within a millimetre of NSMT1 and observing the resulting electrons 0.44 m distant (**see second article by Bryan for details of detector and calibration**), a lensless electron microscope is formed, commonly known as a point projection microscope, here referred to as fs-ePPM to denote the femtosecond electron imaging capability. The magnification is defined by the ratio of the source-target and source-detector distances, and factors of more than 1000 are routine.

An optical microscope image of NSMT2 is presented in fig 2(a), along with fs-ePPM images. As discussed elsewhere, election images are recorded with a microchannel plate pair, a phosphor screen and a 16-bit camera. Figure 2(b) is such an image, recorded when the laser pulse arriving at NSMT2 is significantly later than the passing electron pulse. The overall shape of the NSMT can be observed, however the resolution is limited by mechanical vibration caused by turbomolecular pumps and residual pointing instability in the laser pulses. Figure 2(c) is recorded when the laser pulse on NSMT2 arrives some 4 picoseconds before the electron pulse, illustrating the key concept of this work. The laser illumination causes localized charging around NSMT2, which as the potential applied is small, remains in the vicinity of the apex then deflects the passing femtosecond electron pulse. As discussed later, the flux in this passing pulse is small, however the Coulomb interaction is so strong that a measurable scattering occurs.

The time-dependent scattering is highlighted by taking a slice through the electron images. Figure 3(a) illustrates the position of the slice, while figure 3(b) shows a colour map of the resulting temporal evolution. It is important to realize that the image recorded at each delay is the result of 5×10^4 laser shots, made possible by the extremely rapid recovery of the charge distribution in both NSMT1 and 2. The apparent spreading of
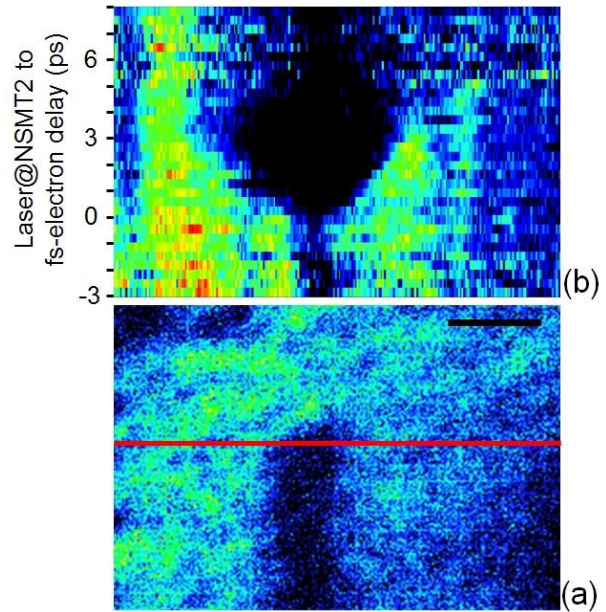
Figure 3. Time-resolved microscopy using femtosecond electron pulses. (a) Apex of NSMT2 (scale bar is 3 micron), and red line indicates slice through time-dependent dataset recorded as the delay between laser pulses illustrated in figure 1 is scanned. (b) Corresponding slices as a function of delay between arrival of laser pulse at NSMT2 and the fs-electron pulse. The charge expansion of the end of the nanotip is cycled for 5×10^4 laser shots and averaged over 500nm in the vertical direction.

the image of NSMT2 is a consequence of the charging of the apex of the tip within hundreds of femtoseconds.

Modelling and e-pulse duration and flux measurement

By carefully determining the magnification (hence source-target distance) and comparing to the resulting image size and flux, we were able to determine the geometry of the NSMT1+2 set-up to within 20 microns. Furthermore, earlier magnification and electron pulse spread measurements allowed the size of the electron emission site to be determined.

An electrostatic model of the NSMT, target and field free flight region to the detector are modelled using Poisson Superfish (Los Alamos Accelerator Code Group), which is then imported into the General Particle Tracer (GPT, Pulsar Physics), used to model charged particle dynamics in EM fields. This is discussed in more detail in the article "Ultrafast electron flux calibration for nanoscale dynamic imaging" also by Bryan.

Figure 4 presents the outcome of these simulations, whereby we make a direct comparison between the electron flux in a series of images as the delay between the laser pulse arrival time at NSMT1 and NSMT2 is varied. As the polarizations of the two laser pulses is perpendicular, we see no emission at NSMT1 from the NSMT2 laser and vice versa. The delay therefore is purely the temporal relation between the arrival times of the laser and electron pulses at NSMT2. Given that the majority of the light passing NSMT2 exits the vacuum chamber, we have also been able to optically measure the delay between the pump and probe laser pulses. This gives a further confirmation of the flight time of the electrons, and is accurate to 5 ps, which is at the limit of the photodiodes and oscilloscope used.

The GPT model allows the inclusion of SC effects when modelling the propagation of femtosecond electron pulses. As we are dealing with very small fluxes, it is possible to treat the electron pulses as 2000 particles with less than unit charge and calculating the 3D SC interaction between them all without approximation. The outcome of such simulations is a pulse
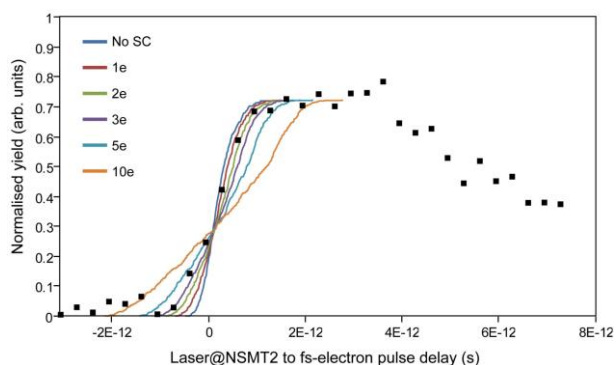
Figure 4. Using GPT space-charge pulse propagation calculations to recover electron flux. The data-points are a sample of the electron flux at the very apex of the image of NSMT2 as a function of time. The zero-delay point is corrected through the use of the optical delay between the two laser pulses and confirmed by the simulations. The cumulative electron flux is compared directly to the sequential image difference. No SC is the case whereby the geometric and bandwidth stretch of the electron pulse limit duration at the target. 1e to 10e are the predictions with full three-dimensional space charge calculations. The electron pulse is represented by 2000 fractional charges. As indicated, the observed pulse rise time is comparable with between one and three electrons per pulse on average.

duration at target, which we convert to a cumulative charge. This treatment is reasonable as the scattering of the electron pulse originating at NSMT1 by NSMT2 is cumulative, that is the influence is time-integrated with a limit specified by the delay between the two laser pulses.

Looking at figure 4 in detail, as the total charge of the electron pulse is varied between no SC (i.e. only limited by the bandwidth of the electron pulse as defined by the pump laser pulse) to 10 electrons (10e) it is clear that this observation is consistent with an electron flux of between one and three electrons per pulse on average. When compared to our electron flux calibration presented elsewhere, this observation is also consistent to ±1 electron. The best fit electron pulses in the presented experimental data have a standard deviation of approaching 100 fs. We are currently analyzing and preparing for publication the characterization of pulses that are significantly shorter.

Conclusions

We have demonstrated femtosecond point-projection microscopy of a nanoscale metal tip illuminated by an ultrafast laser pulse. Using two nanotips, one as a source and the second as a target, we make use of the very rapid (i.e non-thermal) nonlinear electronic response of such objects to not only determine the duration of the electron pulse, but also the number of electrons present on average. Such a measurement will open the door to the observation of faster processes in fs-ePPM, characterization of photonic compression of electron pulses, an improved understanding of nanophotonics and the further use of femtosecond electron pulses for microscopy in atom scale electronics, chemistry and biology.

Acknowledgements

References

1. A. H. Zewail, Science 328 p187–93 (2010)

2. G. Sciaini and R. D. J. Miller Rep. Prog. Phys. 74 096101 (2011)

3. D. J. Flannigan and A. H. Zewail Acc. Chem. Res. 45 p1828–39 (2012)

4. R. D. J. Miller, Science 343 p1108-16 (2014)

5. M. Muller, A. Paarmann and R. Ernstorfer, arxiv.org 1405.4992 (2014)

6. M. Gulde et al, Science 345 200-204 (2014)

7. A. R. Bainbridge and W. A. Bryan, New J. Phys. **16** 103031 (2014)

8. F. O. Kirchner et al, Nat. Photonics 8 p52–57 (2014)

9. E. Quinonez, J. Handali and B. Barwick, Rev. Sci. Instrum. 84, 103710 (2013)

10. P. Baum, J. Phys. B: At. Mol. Opt. Phys. 47 124005 (2014)